

Beneficial Investigation of Extended-Range Electric Powertrains with Dual Motor Input and Automated Manual Transmission

Cong Thanh Nguyen, Paul D. Walker, Nong Zhang*

School of Mechanical and Mechatronic Engineering, Faculty of Engineering and Information Technology,
University of Technology Sydney, 15 Broadway, 2007 Ultimo, NSW, Australia

* Corresponding author: Nong Zhang

Email address: Nong.Zhang@uts.edu.au

Abstract

With the functions of plug-in charging and on-board electric generation, extended-range electric vehicles (EREVs) can overcome limitations of pure electric vehicles, including short driving range, large battery requirement, and charging interruption on road. Current EREVs mainly employ a propulsion motor and single-speed transmission, which suffer poorer dynamic performance and lower motor efficiency. Therefore, this research proposes two novel EREV powertrains to overcome the above shortcomings. Both designs consist of the same electric drivetrain with dual propulsion motors and four-speed automated manual transmission. The fundamental difference is from the range extenders that connect the engines to the electric drivetrains in different ways. First, the parallel engine powertrain (PEP) connects the engine mechanically through a frictional clutch. Second, the series engine powertrain (SEP1) features the engine-generator unit for electric generation. The performance improvements of the proposed configurations are compared to the traditional single motor-series engine powertrain (SEP0). Based on dynamic requirements, the parameters of powertrain components are designed to ensure all configurations equivalently. The model predictive control-based energy management strategy with the forward dynamic programming solver is then designed. Performance indexes for comparison include electric consumption, fuel consumption and gas emissions (CO, HC, NO_x, and PM). Simulation results in the driving cycle CBDC and ECE×5 show that, compared to the traditional SEP0, the SEP1 improves all performance indexes significantly, while the PEP decreases fuel consumption further but increases most noxious exhaust emissions considerably.

Keywords: Extended-range electric vehicles (EREVs), Dual motor-series engine powertrain, Dual motor-parallel engine powertrain, Automated manual transmission, Energy management strategy, Model predictive control.

1. Introduction

Environmental pollution and fossil fuel shortage have encouraged the rapid development of electrified vehicles. Currently, driving range limitation and high battery cost are primary obstacles to popularize electric vehicles (EVs), especially for commercial purposes. In extended-range electric vehicles (EREVs), the on-board electricity generation is realized by employing a range extender, normally formed by an engine generator unit (EGU). The following advantages of the EREVs are achieved as a result: (1) no need for large battery, so comparatively lower initial expense; (2) no limitation of driving range per charge with the support of the range extender; (3) no interruption for plug-in charging on road; (4) no need for public charging infrastructures. (5) Waste heat from the engine can also be used to warm up the vehicles in cold weather. Therefore, the EREVs can be considered as a better alternative to transfer from conventional vehicles to EVs for a range of consumers.

Powertrain configuration is a decisive factor that determines vehicle operations, including dynamic performance and energy efficiency. The EREV configuration can be separated into electric drivetrain (ED) and range extender (RE). The ED operates with electric motor propulsion, while the RE generates on-board electricity. The produced electricity is prioritized for motor propulsion, and then for battery charging. Previous works on EREV configuration have focused on the proposal of different RE alternatives, such as micro-turbine, Wankel engine, and over-expanded cycle engine [1], external combustion gas turbine [2], and fuel cell [3, 4]. On the other hand, the ED mainly employs a single-speed transmission and big propulsion motor [1-4]. The single-speed transmission limits vehicle dynamic performances such as maximum speed, acceleration, and grade. With the single-speed transmission, the motor also suffers poor efficiency at low torque and low speed. Moreover, the single motor frequently operates with small torque utilization factors, which reduce motor efficiency [5]. From all above analyses, this research will address the current problems of the EREV configuration for commercial bus purposes.

The EREV can be considered as an electric vehicle with the additional function of on-board electric generation. Thus, the ED configuration is applied to all developments of electric vehicles. Firstly, multi-speed transmission can avoid motor working in the region of low speed and low torque, so improve efficiency significantly [6]. Therefore, the implement possibility of all current transmissions has been studied, including automated manual transmission (AMT), dual clutch transmission (DCT), automatic transmission (AT), and continuously variable transmission (CVT). Compared to other transmissions, the CVT has lower efficiency due to the different operating principle. Thus, taking the CVT efficiency into account, the overall efficiency of the single-speed transmission is even higher than the CVT [7]. The applications of 2-speed DCT and AT to passenger electric powertrains were

demonstrated to improve motor efficiency [6, 8]. However, both DCT and AT with planetary gears suffer complicated structure, sophisticated control, and high cost. In contrast, the AMT achieves the best balance of manufacturing cost, energy efficiency, and dynamic ability. The gear shifting control of electric vehicles using the AMT was investigated to obtain shifting smoothness [9, 10]. However, the emergence of the torque interruption during gear shifting is unavoidable [9, 10].

Recently, some researchers have proposed electric powertrains with two motor input for passenger vehicles. With two independent power flows through the transmission, the powertrains can eliminate the torque interruption during shifting [11-13]. Moreover, the downsized motors can operate independently or cooperatively with higher torque utilization factors than the single motor [5, 12, 13]. Consequently, the motors can work more frequently in their peak efficiency regions. Liang [11-13] designed the first main motor connects to 3-speed AMT, while the second auxiliary motor links to single-speed AMT. The role of the auxiliary motor mainly operates during the high power demand and gear shifting, which results in the limitation of overall efficiency. Wu [5] proposed dual motor powertrain, which connects each motor to a fix gear ratio. Thus, the powertrain can avoid the shifting requirement, but the motor efficiencies are still restricted. Applying the idea of dual motor input and multi-speed AMT of passenger vehicles, powertrain designs for commercial buses are proposed in this research.

The minimization of fuel consumption and exhaust emissions are the primary objectives of energy management strategies (EMSs). Generally, EMSs can be classified into local and global optimizations. Dynamic programming is the most common method used in global optimizations [14, 15]. Due to computationally intensive nature, global optimizations are mainly used as benchmarks for evaluating other real-time methods [16] or new powertrain designs [17]. Local EMSs can be separated further into rule-based EMSs and optimization-based EMSs. Since rule-based EMSs mostly rely on expert knowledge, they are challenging to obtain optimal results [18]. Besides, the recommendation and calibration of control rules require a lot of time and investment. On the other hand, optimization-based EMSs can optimize cost functions simultaneously. Most recent studies have concentrated on optimization-based EMSs, including Pontryagin's minimum principle [15], equivalent consumption minimization strategy [19], artificial neural network [20], model predictive control (MPC) [21, 22]. With the predicted information of driving conditions from the global positioning system, the MPC-base EMSs can nearly obtain global optimization results [21, 22]. Dynamic programming was generally selected as a solver to optimize cost function in the time horizon [22, 23].

From the literature review of current EREVs, this research proposes two novel powertrains to increase energy efficiency as well as decrease exhaust emissions of EREVs. The emission gases taken into account consist of

hydrocarbon (HC), carbon monoxide (CO), nitrogen oxides (NO_x), and particulate matter (PM). On the one hand, both proposed powertrains include the same ED of dual propulsion motors and four-speed AMT. The AMT can improve vehicle dynamic performances and motor efficiencies. The dual downsized motors can also operate with higher efficiency than the single motor. On the other hand, the recommended powertrains feature fundamentally different RE layouts. The first RE connects the engine to the ED in parallel (parallel engine powertrain), while the second RE connects in series (series engine powertrain). The fuel consumption and gas emissions of each powertrain layouts will be investigated in detail. The performance improvements are evaluated in comparison with the traditional single motor-series engine powertrain. Besides, the MPC-based energy management strategy is selected to use in this research.

The remainder of this paper is divided into the following sections. The first section proposes two novel configurations, operation analysis, and parameter selection for the EREVs. In the next section, mathematical models are presented, including the models of the powertrain system, vehicle dynamics, engine, and battery. A MPC-based energy management strategy with the forward dynamic programming solver is then described. Simulation results are analyzed in the next section, and our conclusions are finally drawn.

2. Powertrain configuration and parameter selection

2.1. Powertrain configuration

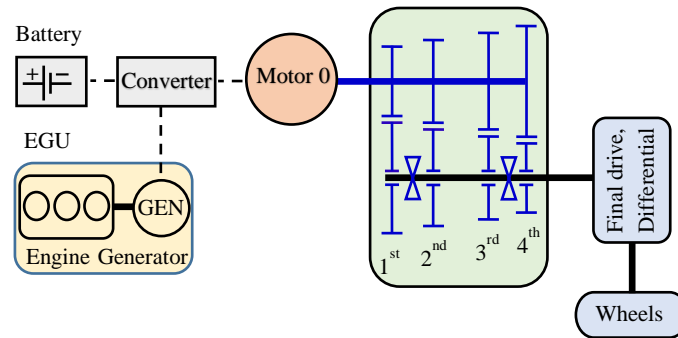


Fig. 1 Configuration of single motor-series engine powertrain (SEP0)

Due to the advantages of simple structure, easy handling, and high transmission efficiency, the series EREV is applied widely in the vehicle market (Fig. 1). The ED with single motor propels the vehicle independently with the electricity provided by the battery. The diesel engine and integrated starter generator compose a RE to supply extra energy if a driving trip exceeds the battery capacity. The single motor drives the vehicle through a four-speed AMT, so both motor efficiency and dynamic ability are improved significantly. However, the torque

interruption during gear shifting produces unwanted jerks, hence reduces vehicle comfort. Besides, the single large motor often operates with low torque utilization factor that lessens motor efficiency.

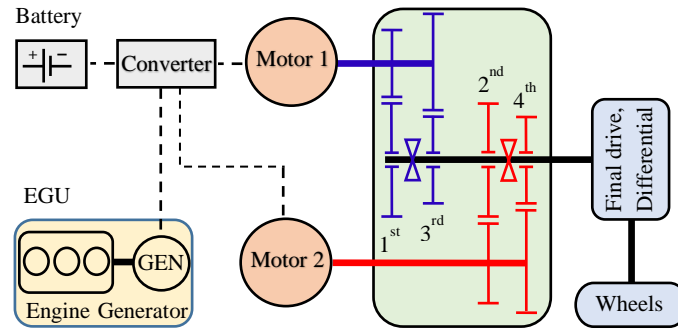


Fig. 2 Configuration of dual motor-series engine powertrain (SEP1)

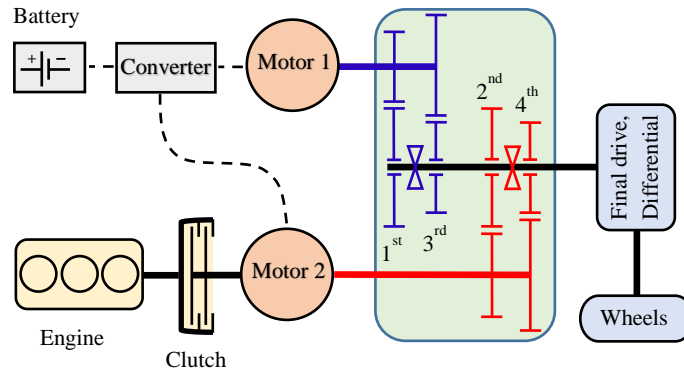


Fig. 3 Configuration of dual motor-parallel engine powertrain (PEP)

To overcome the shortcomings of the conventional series EREV, this research proposes two novel configurations for the EREVs (Fig. 2, Fig. 3). Each configuration consists of a four-speed AMT with two input shafts connect to odd gears (1st and 3rd gears) and even gears (2nd and 4th gears), respectively. Besides, dual downsized motors propel the vehicle with two independent power flows through the respective input shafts. Therefore, the existence of one power flow during the gear shifting can compensate for the power demand and eliminate the torque interruption. Furthermore, in low and mild torque requirement, the downsized motors can work with higher torque utilization factors, so increase their efficiency. The connections of diesel engines to the rest of powertrains create two different RE designs. One design has a form of the series EREV, so the engine transforms fuel energy into electric energy to charge the battery or supply to the dual motors (Fig. 2). Another design has a pattern of the parallel EREV that mechanically links the engine to one input shaft via a frictional clutch (Fig. 3). This research investigates the performance of the two proposed configurations in comparison with the conventional series EREV. Based on powertrain composition, this research sequentially names the three

layouts as single motor-series engine powertrain (SEP0) (Fig. 1), dual motor-series engine powertrain (SEP1) (Fig. 2), and dual motor-parallel engine powertrain (PEP) (Fig. 3).

The SEP1 can operate in three modes, specifically motor 1 only, motor 2 only, and two motors cooperatively. In contrast, with the engine connects in parallel, the PEP has a total of 8 modes, including 3 EV modes, engine mode, series hybrid mode, and 3 parallel hybrid modes (Tab. 1). The EV modes of the PEP are similar to the SEP1, while the parallel modes are the combination of the engine and motor 1, or motor 2, or both motors. Compared to the SEP0, the SEP1 and PEP can improve overall efficiency in two ways. The downsized motors can operate separately or concurrently with higher torque utilization factors. Secondly, with more working modes, 3 for the SEP1, and 8 for the PEP, the power sources have more possibilities to run in their relatively high efficient regions.

Considering the engine operation, the SEP0 and SEP1 have the engines in series connection, which is beneficial in simple structure, easy control, and peak engine efficiency. However, the series energy transformation from fuel to electricity suffers energy loss in related devices: the generator, battery, inverter, and motor. Conversely, the PEP can reduce the loss of energy conversion by the direct drive of the engine. Nevertheless, the mechanical link to driven wheels requires the engine of the PEP to work in wide ranges of speed and torque. Thus, the optimization of exhaust emissions and fuel consumption is difficult to achieve. The PEP is also disadvantageous in complex structure and handling.

Tab. 1 Operating modes of the PEP

Mode	Description		
	Engine /Clutch	Motor 2/Even Synchronizer	Motor 1/Odd Synchronizer
EV	×/×	×/×	±/●
	×/×	±/●	×/×
	×/×	±/●	±/●
Engine	+/●	×/●	×/×
Series hybrid	+/●	−/×	±/●
Parallel hybrid	+/●	×/●	±/●
	+/●	±/●	×/×
	+/●	±/●	±/●

Description: ‘±’ means positive or negative power; ‘●’ means engaged clutch or synchronizer; ‘×’ means power off, disengaged clutch or synchronizer.

2.2. Parameter selection

Since parameter optimization is out of the scope of this research, powertrain parameters are estimated based on the vehicle operation in boundary conditions, namely maximum acceleration, grade, and speed. Besides, the parameters of the SEP0 will be calculated in detail to illustrate the general principle of the design process. The parameters of the SEP1 and PEP will be then determined to guarantee all configurations to obtain equivalent dynamic performances.

Acceleration and grade ability are the base for determining motor power. For acceleration performance, the power to speed up from 0 to v_f in the duration of t_a is obtained as [24]:

$$P_{m0}^{acc} = \frac{\delta M}{2t_a} (v_f^2 + v_b^2) + \frac{2}{3} M g f_r v_f + \frac{1}{5} \rho_a C_d A_f v_f^3 \quad (1)$$

Where M is the gross mass of vehicle, δ is the combined rotational inertia coefficient, t_a is the acceleration time, v_f is the final speed, $v_b = v_f / i_m$ is the base speed, i_m is the speed ratio, g is the gravitational acceleration, f_r is the tyre rolling resistance, C_d is the aerodynamic drag coefficient, ρ_a is the air density, A_f is the vehicle front area.

For grade ability, the power to propel the vehicle in the maximum inclination can be expressed as:

$$P_{m0}^{grade} = \left(M g \sin \varphi_{max} + M g f_r \cos \varphi_{max} + \frac{1}{2} \rho_a C_d A_f v_\varphi^2 \right) v_\varphi \quad (2)$$

The peak power of motor 0 is selected as:

$$P_{m0} = \max(P_{m0}^{acc}, P_{m0}^{grade}) \quad (3)$$

Since the motors of the SEP1 and PEP connect to the consecutive gears of the AMT, the motors are set to be the same size and have a haft power of motor 0. The detail specifications and efficient maps of the motors are presented in Tab. 3 and Fig. 4a, b [25], respectively.

With the series engine connection of the SEP0 and SEP1, the engine only provides electricity for charging the battery or driving the motors. For the PEP, the engine also supports the motors to propel the vehicle when the battery is exhausted. Therefore, dynamic performance does not really relate to engine parameters. The engine selection actually depends on battery size, driving range per charge, and control strategy. With the primary purpose of configuration comparison, a 2.5L diesel engine is chosen for all configurations. The generator of the SEP0 and SEP1 is selected to ensure both the engine and generator to work in their peak efficiency regions. The detail specifications of the engine and generator are presented in Tab. 3. The efficient map of the generator, fuel consumption and emission maps of the engine are shown in Fig. 4c-h [25].

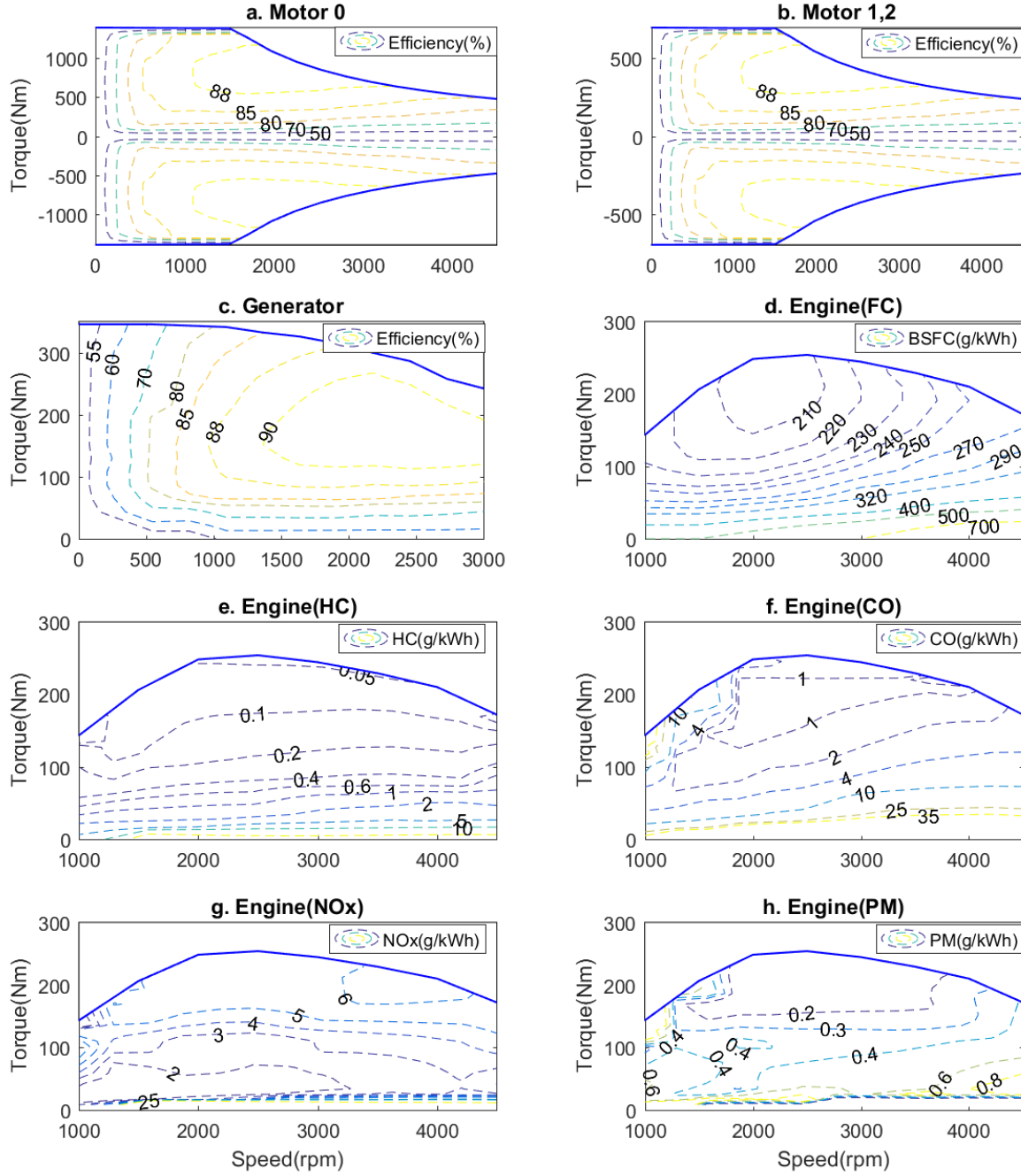


Fig. 4 Operating maps of the motor, generator, and engine [25]

The AMT and final drive are designed to guarantee vehicle operation at maximum grade and speed. The vehicle acceleration is presumed to be zero in these conditions. For this reason, the vehicle load torque includes of rolling resistance, inclination resistance, and aerodynamic drag as:

$$T_{load} = \left(Mg \sin \varphi + Mgf_r \cos \varphi + \frac{1}{2} \rho_a C_d A_f v^2 \right) r_t \quad (4)$$

Where is φ is inclination angle, r_t is the wheel radius.

The lowest gear ratio is identified at the grade of 50% and the constant speed of 10 km/h as:

$$T_{m0}^{\max}(v_{\varphi_{\max}})i_1i_0\eta_{mw} \geq T_{load}(\varphi_{\max}, v_{\varphi_{\max}}) \quad (5)$$

Where φ_{\max} is the maximum grade, $v_{\varphi_{\max}}$ is the corresponding speed at the grade of φ_{\max} , i_1 is the 1st gear ratio, i_0 is the gear ratio of final drive, $T_{m0}^{\max}(v_{\varphi_{\max}})$ is the corresponding torque of motor 0 at the speed $v_{\varphi_{\max}}$, η_{mw} is the transmission efficiency from motor 0 to the driven wheels.

The highest velocity of 80 km/h corresponds to the maximum motor speed and the highest gear of the AMT (4th gear) as:

$$i_4i_0 \leq \frac{3.6\pi r_t N_{\max}}{30v_{\max}} \quad (6)$$

Where N_{\max} is the maximum speed of motor 0.

The traction torque at the highest velocity needs to be rechecked as:

$$T_{m0}^{\max}(v_{\max})i_4i_0\eta_{mw} \geq T_{load}(\varphi_{v_{\max}}, v_{\max}) \quad (7)$$

Using the constraints (5-7), the ratio of the final drive, maximum and minimum ratios of the AMT can be determined. Besides, the geometrical gear step is used to select the ratios of the intermediate gears [26].

The principle to select the gear ratios of the SEP1 and PEP is similar to the SEP0. However, both the motors will operate at the maximum inclination and acceleration while only motor 2 will propel in the 4th gear at the highest velocity. Finally, the gear ratios and dynamic performances of all configurations are shown in Tab. 2. The results consist of the maximum vehicle speed (v_{\max}), grade ability (φ_{\max}), and velocity after 10s acceleration (v_{\max}^{10s}). The calculation results show that the SEP0 and SEP1 perform similarly in all conditions. Without the engine support, the achievement of the PEP will be identical to the SEP1. Nevertheless, the parallel engine connection can help the PEP to achieve better grade and acceleration capability.

Tab. 2 Dynamic performances of three configurations

	SEP0	SEP1	PEP
$[i_1/i_2/i_3/i_4]$	5.0/3.8/2.8/2.1	5.9/4.2/3.0/2.1	
i_0	5.2		
$v_{\max}(km/h)$	81.7		
$\varphi_{\max}(\%)$	47.3	47.2	53.1
$v_{\max}^{10s}(km/h)$	56.6	56.3	61.8

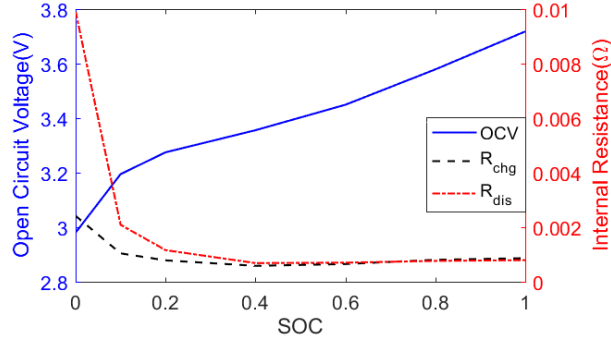


Fig. 5 Battery internal resistances and open circuit voltage [25]

The battery includes 200 lithium-ion cells in series connection. Each cell has the capacity of 180Ah, the nominal voltage of 3.4V. Battery internal resistances and open circuit voltage are presented in Fig. 5 [25]. The parameters of the battery pack are shown as in Tab. 3.

Tab. 3. Specifications of the vehicle and proposed powertrain

	Parameters	Value
Vehicle	Gross weight	15000 kg
Battery	Battery type	Lithium ion
	Nominal voltage/Capacity	680 V/180 Ah
Engine	Engine type	Diesel, 2.5L
	Maximum power/Maximum speed	88 kW/4500 rpm
Motors	Motor type	PMSM
	Peak powers of motor 0/1/2	224/112/112 kW
	Max speed/Base speed	4500/1500 rpm
Generator	Generator type	PMSM
	Peak power	76 kW
	Max speed/Base speed	3000/1000 rpm

3. Mathematical model

3.1. Powertrain model

The motors and/or engine supply the required torque to the driven wheels during the acceleration process. In contrast, the motors regenerate braking energy to save in the battery. The mechanical braking system supports the motors to decelerate the vehicle safely. In general, the required torque in the driven wheels of the SEP0, SEP1, and PEP are sequentially presented as in (8)-(10):

$$T_w = T_{m0} i_{AMT} i_0 \eta_t + T_{bF} \quad (8)$$

$$T_w = (T_{m1}i_{Odd} + T_{m2}i_{Even})i_0\eta_t + T_{bF} \quad (9)$$

$$T_w = (T_{m1}i_{Odd} + T_{m2}i_{Even} + T_e i_{Even})i_0\eta_t + T_{bF} \quad (10)$$

Where T_{mi}, T_e are the torque of the motor $i(i = 0,1,2)$ and engine; $i_{AMT}, i_{Odd}, i_{Even}$ are gear ratio of the AMT, odd gear, and even gear, respectively; η_t is the efficiency of the transmission system; T_{bF} is the front braking torque which equals zero in driving condition, while the rear braking torque is provided by the motors.

3.2. Vehicle dynamic model

From the longitudinal dynamics, the required torque is consisted of the acceleration torque and load torque as:

$$T_w = \left(\delta M \frac{dv}{dt} + Mg \sin \varphi + Mgf_r \cos \varphi + \frac{1}{2} \rho_a C_d A_f v^2 \right) r_t \quad (11)$$

The total braking torque is generally allocated to all wheels to fully use the tire-to-road adhesion as well as improve vehicle stability. The ideal allocation of the front and rear braking forces (Fig. 6) is expressed as [27]:

$$F_{xR} = \frac{Mg}{2h_g} \left(\sqrt{b^2 + \frac{4h_g L}{mg} F_{xF}} - b \right) - F_{xF} \quad (12)$$

Where F_{xF}, F_{xR} are the braking force of front wheels and rear wheels ($T_{bF} = F_{xF}r_t, T_{bR} = F_{xR}r_t$), h_g is the height of gravitational centre, L is the wheel base, b is the distance from the gravitational centre to the rear axle.

Since only the rear braking power can be recovered, the ideal allocation wastes a large amount of energy in the front wheels. Therefore, the ideal torque distribution is only applied in the emergency braking process. In the slight and medium braking requirement, using only rear braking torque can satisfy braking requirements and maximize the energy recovery. Consequently, the actual braking distribution is detailed in Fig. 6.

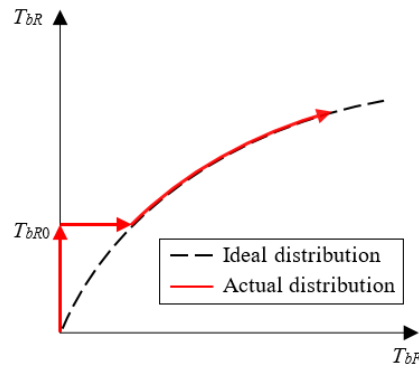


Fig. 6 Distribution of braking torques

3.3. Engine model

Since the engine dynamics is out of this research, the simplified engine model mainly concerns the fuel consumption and emission as:

$$\dot{F}C = \frac{\mu_e}{\rho_f} P_e \quad (13)$$

$$\dot{G}E = \mu_{EG} P_e \quad (GE = \{HC, CO, NOx, PM\}) \quad (14)$$

Where FC is the fuel consumption, GE is the gas emission (HC, CO, NOx, and PM), μ_e is the fuel rate, ρ_f is the fuel density, and μ_{EG} is the emission rate, and P_e is the engine power. The fuel rate and emission rate are interpolated from the engine maps in Fig. 4.

3.4. Battery model

This research neglects the effect of battery temperature and age. The battery model is simplified using the open-circuit voltage in series. Therefore, the battery SOC is computed as [28]:

$$\dot{SOC} = -\frac{(U_{OC} - \sqrt{U_{OC}^2 - 4P_{bat}R_{bat}})}{2C_{bat}R_{bat}} \quad (15)$$

Where SOC is the battery state of charge, U_{OC} is the open circuit voltage, R_{bat} is the internal resistance, C_{bat} the battery capacity, P_{bat} the battery power, that is calculated for the SEP0 as in (16) and for the SEP1 and PEP as in (17):

$$P_{bat} = P_{m0}(\eta_{m0}\eta_c)^{-sign(P_{m0})} \quad (16)$$

$$P_{bat} = (P_{m1}\eta_{m1}^{-sign(P_{m1})} + P_{m2}\eta_{m2}^{-sign(P_{m2})})\eta_c^{-sign(P_{m1}\eta_{m1}^{-sign(P_{m1})} + P_{m2}\eta_{m2}^{-sign(P_{m2})})} \quad (17)$$

Where P_{mi} and η_{mi} are the power and efficiency of the motor i ($i = 0,1,2$), η_c is the converter efficiency.

4. Energy management strategy

The objective of the energy management strategy is to minimize fuel consumption, emissions and guarantee other dynamic performances. In this research, the EMS considers the control system at the supervisory level that calculates the optimum values of powertrain operation. The optimum values are then used as references for the tracking control in the low-level control. The EMS at the supervisory level is a nonlinear optimization problem that is solved here by the model predictive control (Fig. 7) [29]. In each time step, the optimal control sequences are determined to minimize the cost function in the prediction time horizon. The first control sequence is then

chosen to apply to the EREV model. The inputs of the MPC controller consists of the required vehicle speed, torque, and other states. The demand speed and torque can be obtained from the driving cycle and calculation, respectively. The other states are the outputs of the EREV model, such as the SOC, gear state... In practical application, the inputs can be provided by the driver model or by using sensors and observers. The outputs are different for each powertrain configuration and are detailed as follows.

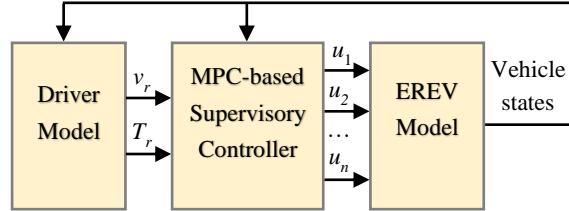


Fig. 7 Framework of the MPC-based energy management strategy

From the previous equations, the control system is modeled as:

$$\begin{cases} \dot{x} = f(x, u, w) \\ y = g(x, u, w) \end{cases} \quad (18)$$

Where $x = SOC$ is the state variable, y is the measured output, u is the control input, $w = [v_r, T_r]^T$ is the disturbance. The selection of the control input and measured output depends on the powertrain configuration. Therefore, the input and output for the SEP0, SEP1, and PEP are respectively presented as in (19), (20), and (21):

$$u = [\omega_e, T_e, T_{m0}]^T, y = [FC, GE, \omega_{m0}, T_g, \omega_g, i_{AMT}]^T \quad (19)$$

$$u = [\omega_e, T_e, T_{m1}, T_{m2}]^T, y = [FC, GE, \omega_{m1}, \omega_{m2}, T_g, \omega_g, i_{odd}, i_{even}]^T \quad (20)$$

$$u = [T_e, T_{m1}, T_{m2}]^T, y = [FC, GE, \omega_e, \omega_{m1}, \omega_{m2}, i_{odd}, i_{even}]^T \quad (21)$$

The EMS requires to use the battery electricity reasonably for the whole driving cycle. However, the optimization in the short time horizon is unable to get global solutions. Therefore, the SOC reference will be added to the cost function for tracking control. The SOC reference is defined according to the intended driving cycle as:

$$SOC_r(m) = SOC_0 - \frac{\sum_{i=1}^m l_i}{L} (SOC_0 - SOC_F) \quad (22)$$

Where SOC_r , SOC_0 , and SOC_F are the reference, initial, and final values of the battery SOC, respectively; l_i is the length of the road part i ; m is the number of road parts that the vehicle has passed, L is the total length of the driving cycle.

Since electricity is much cheaper than fuel, the battery is used as much as possible at the end. Therefore, the EMS is trivial if the battery can cover all the expected energy. Otherwise, the EMS needs to balance between electricity and fuel consumption. The proposed objective function here mainly consists of fuel consumption, the

penalty of SOC deviation. Besides, the regular torque and state changes of the engine and motors are penalized in the cost function to guarantee the practical operation. Consequently, the cost function of the MPC is expressed as in (23) for the SEP0 and in (24) for the SEP1 and PEP.

$$J = \sum_{k=m}^{m+p} (FC(k) + \rho_{SOC}|SOC(k) - SOC_r(k)| + \rho_{Se}|S_e(k) - S_e(k-1)| + \rho_{Te}|T_e(k) - T_e(k-1)| + \rho_{Sm0}|S_{m0}(k) - S_{m0}(k-1)| + \rho_{Tm0}|T_{m0}(k) - T_{m0}(k-1)|) \quad (23)$$

$$J = \sum_{k=m}^{m+p} (FC(k) + \rho_{SOC}|SOC(k) - SOC_r(k)| + \rho_{Se}|S_e(k) - S_e(k-1)| + \rho_{Te}|T_e(k) - T_e(k-1)| + \rho_{Sm1}|S_{m1}(k) - S_{m1}(k-1)| + \rho_{Tm1}|T_{m1}(k) - T_{m1}(k-1)| + \rho_{Sm2}|S_{m2}(k) - S_{m2}(k-1)| + \rho_{Tm2}|T_{m2}(k) - T_{m2}(k-1)|) \quad (24)$$

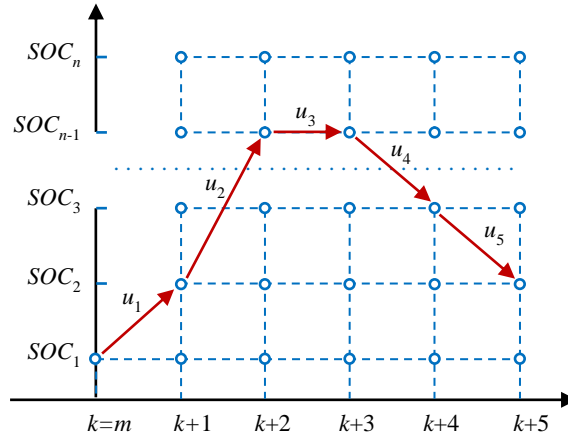


Fig. 8 Architecture of the dynamic programming solver

Where p is the prediction time horizon, $S_i (i = e, m0, m1, m2)$ is the state of the component i ($S_i = 1$ if the component is on, $S_i = 0$ if the component is off), $\rho_i (i = SOC, Se, Sm0, Sm1, Sm2, Te, Tm0, Tm1, Tm2)$ is the penalty factor.

Then the optimal problem is constructed as:

$$\min_{\substack{SOC_{min} \leq SOC \leq SOC_{max} \\ \omega_i^{min} \leq \omega_i \leq \omega_i^{max}, T_i^{min} \leq T_i \leq T_i^{max}}} J(u) \quad (25)$$

This research uses the forward dynamic programming as an MPC solver which is illustrated in Fig. 8. The battery SOC is selected as a state variable that changes in a narrow range in the time horizon of 5s. As a result, the possible SOC range in each step can be divided into a small grid, while the number of the SOC element is limited. Therefore, the DP solver can calculate the optimal results accurately in the acceptable time requirement.

At time point m , the MPC uses the forward DP solver to determine the control sequences $[u_1 u_2 \dots u_5]^T$ in the time horizon (Fig. 8). Then, the first control sequence u_1 will be selected to apply to the EREV model.

5. Simulation results

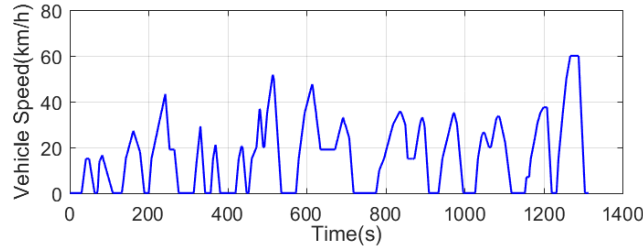


Fig. 9 Chinese bus driving cycle

Simulation models are developed in Matlab and are based on the mathematic model and energy management strategy in the previous sections. Since the proposed configurations aim for bus applications, the powertrain performance is assessed in two driving cycles, specifically the Chinese bus driving cycle (CBDC) (Fig. 9) [30] and the urban driving cycle (ECE15) (Fig. 13) [31]. Besides, depending on the battery capacity and travel length, the operation of the EREVs can be divided into two conditions: electric driving and hybrid driving. In electric driving, motors drive the vehicle without engine support, which results in the identical operation of the SEP1 and PEP. In hybrid driving, the engine keeps the role in generating electricity in all configurations or mechanically drives the vehicle in the PEP.

Fig. 10 compares the performance of the proposed configurations in the electric driving condition in the CBDC. Without fuel consumption, the EMS objective is to minimize electricity consumption with some dynamic constraints. Firstly, the proper gear selection can improve motor efficiency, but the frequent gear changes need to be limited. Consequently, Fig. 10a, b show the reasonable numbers of gear shifting, 51 of the SEP0, and 42 of the SEP1 and PEP. Secondly, the motor torques are required to avoid oscillations with large magnitudes (Fig. 10c, d). In the efficiency map, the working point is determined by the motor speed and torque. With two motor sizes, the left y-axis corresponds to the torques of motor 1 and 2, while the right y-axis corresponds to the torque of motor 0 (Fig. 10e). The remarkable result to emerge from the motor working points is that motor 1 and motor 2 work in the peak efficiency region much more frequent than motor 0. Hence, the efficiencies of the dual motors are improved significantly. Especially, motor 1 operates at a mean efficiency of 72.8%, while motor 1 and motor 2 acquire means of 81.8% and 76.3%, respectively. The efficiency improvement results from the ability to enhance

the torque utilization factors of two downsized motors. Finally, Fig. 10f emphasizes the striking reduction of 7.4% in electricity consumption of the SEP1 and PEP (7.18 kWh) in comparison with the SEP0 (7.75kWh).

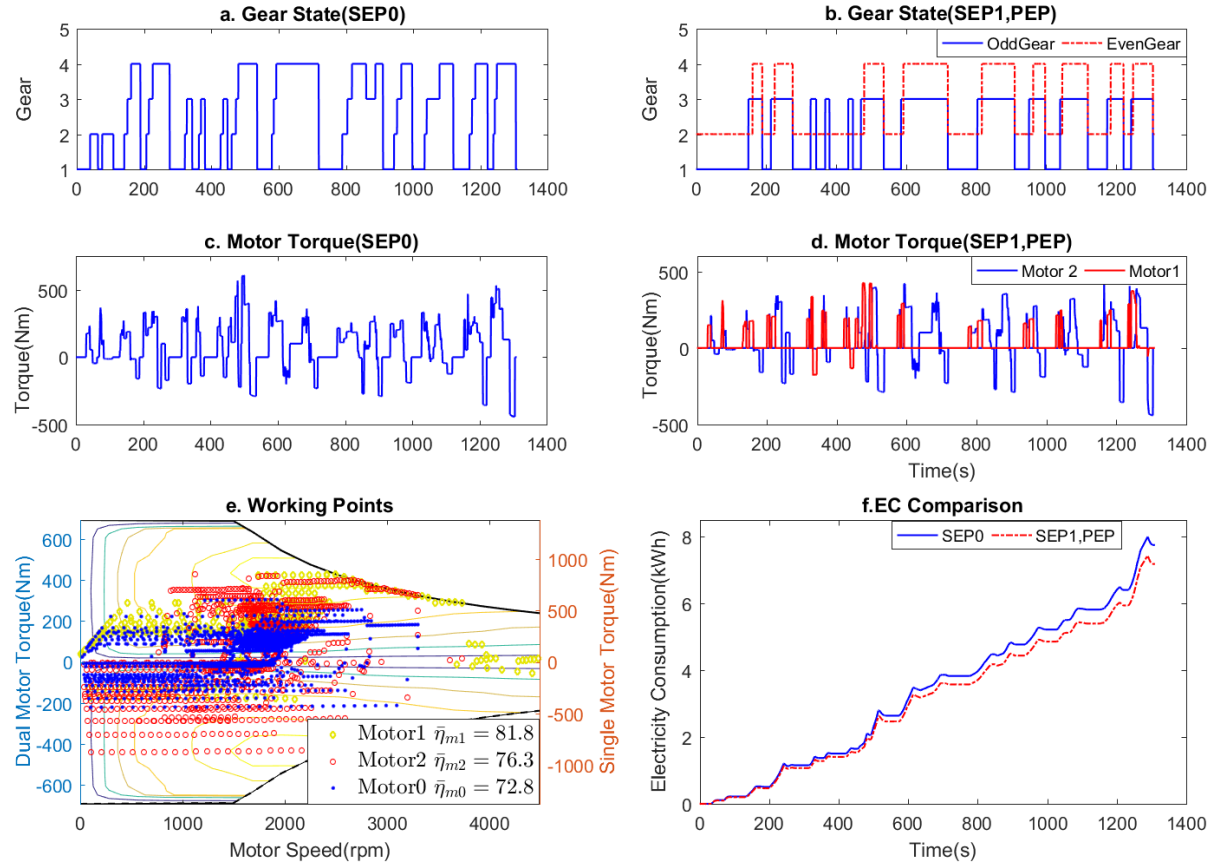


Fig. 10 Operation comparison in electric driving condition

Fig. 11 compares the performances of the proposed configurations in the hybrid driving condition in the CBDC. The proportion of fuel and electricity consumption here depends on the rest of the battery SOC and travel length. In contrast to the electric driving condition, this section investigates powertrain performances when fuel is the primary energy to propel the vehicle. Therefore, the battery is set at a low SOC range from 0.32 to 0.3. The proposed SOC reference is shown in Fig. 11e. With engine connection in series, the motors and AMT transmissions of the SEP0 and SEP1 operate similarly as in the electric driving. Besides, the engines can run independently from the driving situation. Thus, the engines work with steady torques and speeds (Fig. 11a, b) in the peak efficiency region (Fig. 11g). For the PEP, the engine can propel the vehicle mechanically or drive the dual motors to generate electricity (Fig. 11c, d). With the constraint of vehicle dynamics, the engine is required to operate with high torque variations (Fig. 11c) and working points in a wider region (Fig. 11h). Therefore, the stable operation of the engine in the series configurations shows a clear advantage over the parallel layout. The SOC tracking control shows all final values close to the minimum of 0.3 (Fig. 11e). Consequently, the efficiency

is determined by the fuel consumption (Fig. 11h). It is evident that the fuel consumption reduces as in the following sequence: the SEP0, SEP1, and PEP. The statistical results are synthesized later.

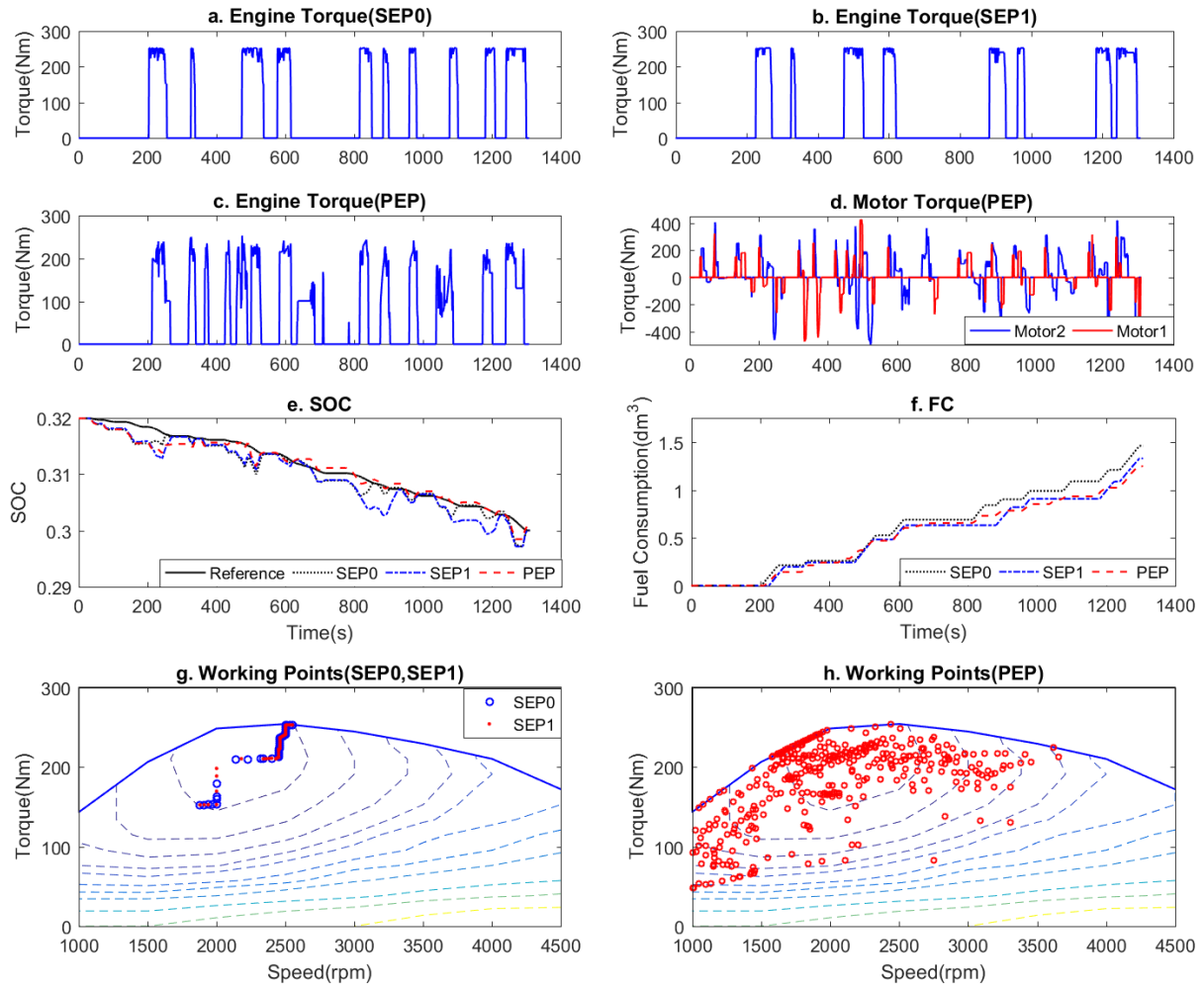


Fig. 11 Operation comparison in hybrid driving condition

Fig. 12 compares the emissions of the engine in the hybrid driving condition in the CBDC. The most striking result to emerge is that the PEP emits much more HC, CO, and PM, but less NO_x than the SEP0 and SEP1. In addition, the emissions of the SEP1 are always less than of the SEP0.

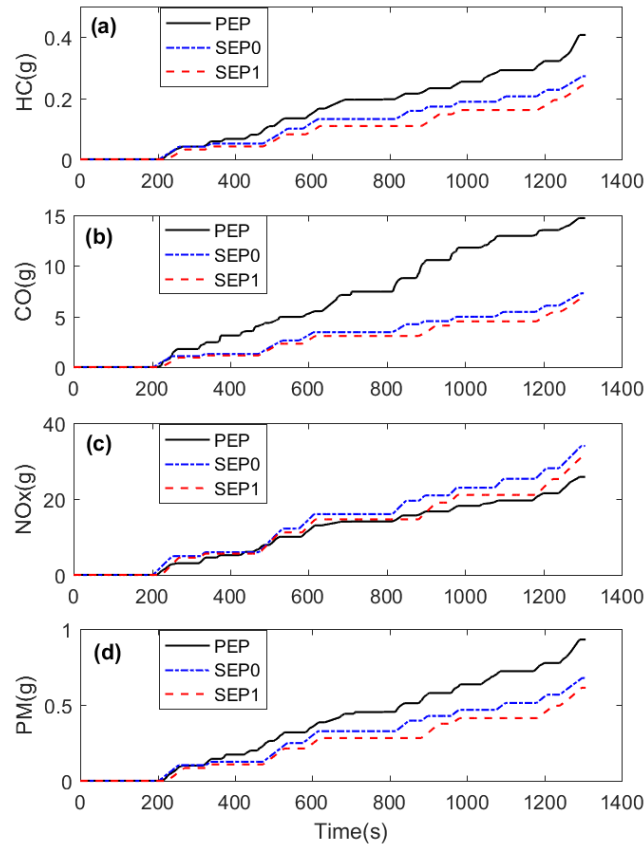


Fig. 12 Comparison of exhaust emissions in hybrid driving condition

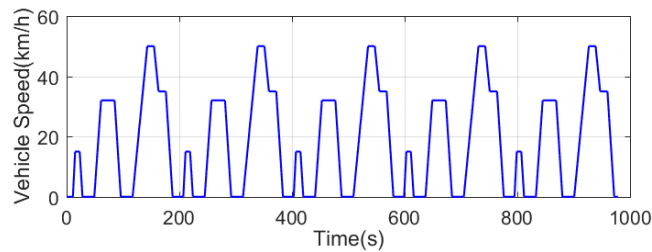
Tab. 4 statistically details performance indexes used to assess the effectiveness of the recommended powertrains in the CBDC. The performance indexes consist of electric consumption (EC), fuel consumption (FC), and gas emissions (HC, CO, NOx, and PM). The achievement of the SEP0 is considered as base values for comparison, in which the positive values present the decrease, while the negative values mean the increase (Tab. 4). In the electric driving condition, the dual motor powertrains (the SEP1 and PEP) reduce EC substantially by 7.4%. Therefore, the electric driving duration in the CBDC with the battery SOC from 0.9 to 0.3 will be 3.45 hours for the SEP0 in comparison with 3.72 hours for the SEP1 and PEP. In the hybrid driving condition, the FC reductions are more remarkable, by 8.9% for the SEP1, and 14.4% for the PEP. However, the exhaust emissions from the engine change in different ways. On one hand, the SEP1 improves all emission indexes considerably by reducing from 7.4% in CO to 10.3% in PM. This is consistent with the fuel consumption and working points of the engine in the series engine powertrains. On the other hand, the PEP only reduces NOx by 24.0% but increases the other gases strikingly by 85.7% HC, 102.1% CO, and 36.8% PM. This results from the engine operation in wide ranges of speed and torque (Fig. 11b). Besides, the fuel and NOx rate maps of the engine are nearly contrary, so a working point obtains peak fuel economy also suffers high NOx emission. Consequently, the NOx increases in the SEP0 and SEP1 are acceptable.

Tab. 4 Comparison of performance indexes in CBDC

Driving condition	Performance index	Configuration			Reduction (%)	
		SEP0	SEP1	PEP	SEP1	PEP
Electric driving	EC (kWh)	7.75	7.18	7.18	+7.4	+7.4
Hybrid driving	FC (dm ³)	1.46	1.33	1.25	+8.9	+14.4
	HC (g)	0.21	0.19	0.39	+9.5	−85.7
	CO (g)	7.29	6.75	14.73	+7.4	−102.1
	NOx (g)	33.97	30.91	25.83	+9.0	+24.0
	PM (g)	0.68	0.61	0.93	+10.3	−36.8

The performance indexes are investigated in another urban driving cycle-ECE15. Since the ECE15 is short, the simulation is conducted in five continuing cycles, namely ECE15×5 (Fig. 13). In general, the calculation results of the indexes in the ECE15×5 are consistent with the outcomes in the CBDC (Tab. 5). Compared to the SEP0, the SEP1 reduces substantially 8.3% EC and 11.5% FC in the electric and hybrid driving, respectively. The emission reductions are more remarkable, from 11.6% in NOx to 25% in HC. For the PEP, the energy economy is even better than the SEP1, with decreases of 8.3% EC and 14.5% FC. Nevertheless, the emissions increase considerably in HC (20%), CO (47.6%), and PM (9.7%), except for NOx.

In summary, compared to the traditional SEP0, the SEP1 improves all performance indexes significantly, while the PEP can decrease fuel consumption further but increases almost exhaust emissions. The main reason behind this is that the engine requires many more gear ratios to be available to ensure that it operates in the most suitable driving ranges. Moreover, as analyzed in the Introduction section, the SEP1 is advantageous in simple structure, control, and easy integration for mass production.

**Fig. 13** ECE15×5 driving cycle

Tab. 5 Comparison of performance indexes in ECE15×5

Driving condition	Performance index	Configuration			Reduction (%)	
		SEP0	SEP1	PEP	SEP1	PEP
Electric driving	EC (kWh)	7.27	6.67	6.67	+8.3	+8.3
Hybrid driving	FC (dm ³)	1.31	1.16	1.12	+11.5	+14.5
	HC (g)	0.20	0.15	0.24	+25.0	−20.0
	CO (g)	6.51	5.21	9.61	+20.0	−47.6
	NO _x (g)	30.29	26.79	24.25	+11.6	+19.9
	PM (g)	0.62	0.50	0.68	+19.4	−9.7

6. Conclusion

To overcome the shortages of current EREVs, this paper studeies two novel dual motor powertrains, including parallel engine powertrain (PEP) and series engine powertrain (SEP1). The effectiveness of the recommended configurations is evaluated in comparison with the traditional single motor-series engine powertrain (SEP0). Based on dynamic performances, parameter designs of system components guarantee all configurations equivalently. The mathematic model and MPC-based energy management strategy are then presented in detail. Powertrain operation is finally simulated in electric driving and hybrid driving condition in two urban driving cycles, the CBDC and ECE×15. Performance indexes used for evaluation consist of electric consumption, fuel consumption, and gas emissions (HC, CO, NO_x, and PM). Simulation results show that dual downsized motors operate in their peak efficiency regions more frequently than the single motor. Consequently, both dual motor powertrains reduce the energy consumption (fuel and electricity) significantly, from 7.4% to 11.5% with the SEP1 and from 7.4% to 14.5% with the PEP. Besides, the SEP1 reduces all gas emissions considerably, from 7.4% in CO to 10.3% in PM in the CBDC and from 11.6% in NO_x to 25% in HC in the ECE×15. In contrast, the PEP increases almost gas emissions strikingly. Moreover, the SEP1 is more advantageous in simple structure, control, and easy integration for mass production.

In summary, the proposed dual motor powertrains can improve the electricity and fuel economy for the EREVs. In comparison with the SEP1, the PEP decreases fuel consumption further but increases almost exhaust emissions remarkably. Additionally, the proposed configurations are not limited for EREV application, the electric drivetrain with dual motor input and four-speed AMT is a great candidate for electric vehicle powertrains.

Acknowledgement

This project was supported by the Australian Research Council under Discovery Early Career Researcher Award (DE0170100134), and University of Technology Sydney.

Appendix I

Abbreviations

AMT	Automated manual transmission
CBDC	Chinese bus driving cycle
EC	Electric consumption
ECE	Urban driving cycle
ED	Electric drivetrain
EMS	Energy management strategy
EREV	Extended range electric vehicle
EV	Electric vehicle
FC	Fuel consumption
HEV	Hybrid electric vehicle
PEP	Parallel engine powertrain
RE	Range extender
SEP	Series engine powertrain
SOC	State of charge

Reference

- [1] J. Ribau, C. Silva, F. P. Brito, and J. Martins, "Analysis of four-stroke, Wankel, and microturbine based range extenders for electric vehicles," *Energy Conversion and Management*, vol. 58, pp. 120-133, 2012, doi: 10.1016/j.enconman.2012.01.011.
- [2] A. Reine and W. Bou Nader, "Fuel consumption potential of different external combustion gas-turbine thermodynamic configurations for extended range electric vehicles," *Energy*, vol. 175, pp. 900-913, 2019, doi: 10.1016/j.energy.2019.03.076.
- [3] T. Zeng *et al.*, "Modelling and predicting energy consumption of a range extender fuel cell hybrid vehicle," *Energy*, vol. 165, pp. 187-197, 2018, doi: 10.1016/j.energy.2018.09.086.
- [4] C. Geng, X. Jin, and X. Zhang, "Simulation research on a novel control strategy for fuel cell extended-range vehicles," *International Journal of Hydrogen Energy*, vol. 44, no. 1, pp. 408-420, 2019, doi: 10.1016/j.ijhydene.2018.04.038.
- [5] J. Wu, J. Liang, J. Ruan, N. Zhang, and P. D. Walker, "Efficiency comparison of electric vehicles powertrains with dual motor and single motor input," *Mechanism and Machine Theory*, vol. 128, pp. 569-585, 2018, doi: 10.1016/j.mechmachtheory.2018.07.003.
- [6] J. Ruan, P. Walker, and N. Zhang, "A comparative study energy consumption and costs of battery electric vehicle transmissions," *Applied Energy*, vol. 165, pp. 119-134, 2016, doi: 10.1016/j.apenergy.2015.12.081.
- [7] T. Hofman, M. Steinbuch, R. M. van Druten, and A. F. A. Serrarens, "Rule-Based Energy Management Strategies for Hybrid Vehicle Drivetrains: A Fundamental Approach in Reducing Computation Time," *IFAC Proceedings Volumes*, vol. 39, no. 16, pp. 740-745, 2006, doi: 10.3182/20060912-3-de-2911.00128.
- [8] J. W. Shin, J. O. Kim, J. Y. Choi, and S. H. Oh, "Design of 2-speed transmission for electric commercial vehicle," *International Journal of Automotive Technology*, vol. 15, no. 1, pp. 145-150, 2014, doi: 10.1007/s12239-014-0016-8.
- [9] W. Mo, P. D. Walker, and N. Zhang, "Dynamic analysis and control for an electric vehicle with harpoon-shift synchronizer," *Mechanism and Machine Theory*, vol. 133, pp. 750-766, 2019, doi: 10.1016/j.mechmachtheory.2018.11.018.
- [10] C.-Y. Tseng and C.-H. Yu, "Advanced shifting control of synchronizer mechanisms for clutchless automatic manual transmission in an electric vehicle," *Mechanism and Machine Theory*, vol. 84, pp. 37-56, 2015, doi: 10.1016/j.mechmachtheory.2014.10.007.
- [11] J. Liang, H. Yang, J. Wu, N. Zhang, and P. D. Walker, "Power-on shifting in dual input clutchless power-shifting transmission for electric vehicles," *Mechanism and Machine Theory*, vol. 121, pp. 487-501, 2018, doi: 10.1016/j.mechmachtheory.2017.11.004.
- [12] J. Liang, H. Yang, J. Wu, N. Zhang, and P. D. Walker, "Shifting and power sharing control of a novel dual input clutchless transmission for electric vehicles," *Mechanical Systems and Signal Processing*, vol. 104, pp. 725-743, 2018, doi: 10.1016/j.ymssp.2017.11.033.
- [13] H. Wu, P. Walker, J. Wu, J. Liang, J. Ruan, and N. Zhang, "Energy management and shifting stability control for a novel dual input clutchless transmission system," *Mechanism and Machine Theory*, vol. 135, pp. 298-321, 2019, doi: 10.1016/j.mechmachtheory.2019.01.032.
- [14] W. Yang, J. Yang, J. Liang, and N. Zhang, "Implementation of velocity optimisation strategy based on preview road information to trade off transport time and fuel consumption for hybrid mining trucks," *IET Intelligent Transport Systems*, vol. 13, no. 1, pp. 194-200, 2019, doi: 10.1049/iet-its.2018.5054.
- [15] N. Guo, J. Shen, R. Xiao, W. Yan, and Z. Chen, "Energy management for plug-in hybrid electric vehicles considering optimal engine ON/OFF control and fast state-of-charge trajectory planning," *Energy*, vol. 163, pp. 457-474, 2018, doi: 10.1016/j.energy.2018.08.116.
- [16] Y. Yang, X. Hu, H. Pei, and Z. Peng, "Comparison of power-split and parallel hybrid powertrain architectures with a single electric machine: Dynamic programming approach," *Applied Energy*, vol. 168, pp. 683-690, 2016, doi: 10.1016/j.apenergy.2016.02.023.
- [17] X. Zhang, C. T. Li, D. Kum, and H. Peng, "Prius+ and volt-: Configuration analysis of power-split hybrid vehicles with a single planetary gear," *IEEE Transactions on Vehicular Technology*, vol. 61, no. 8, pp. 3544-3552, 2012, doi: 10.1109/TVT.2012.2208210.
- [18] W. Enang and C. Bannister, "Modelling and control of hybrid electric vehicles (A comprehensive review)," *Renewable and Sustainable Energy Reviews*, vol. 74, pp. 1210-1239, 2017, doi: 10.1016/j.rser.2017.01.075.
- [19] A. Sciarretta, M. Back, and L. Guzzella, "Optimal control of parallel hybrid electric vehicles," *IEEE Transactions on Control Systems Technology*, vol. 12, no. 3, pp. 352-363, 2004, doi: 10.1109/tcst.2004.824312.

- [20] S. Xie, X. Hu, S. Qi, and K. Lang, "An artificial neural network-enhanced energy management strategy for plug-in hybrid electric vehicles," *Energy*, vol. 163, pp. 837-848, 2018, doi: 10.1016/j.energy.2018.08.139.
- [21] S. Zhang, R. Xiong, and F. Sun, "Model predictive control for power management in a plug-in hybrid electric vehicle with a hybrid energy storage system," *Applied Energy*, vol. 185, pp. 1654-1662, 2017, doi: 10.1016/j.apenergy.2015.12.035.
- [22] P. Shen, Z. Zhao, X. Zhan, J. Li, and Q. Guo, "Optimal energy management strategy for a plug-in hybrid electric commercial vehicle based on velocity prediction," *Energy*, vol. 155, pp. 838-852, 2018, doi: 10.1016/j.energy.2018.05.064.
- [23] G. Li, J. Zhang, and H. He, "Battery SOC constraint comparison for predictive energy management of plug-in hybrid electric bus," *Applied Energy*, vol. 194, pp. 578-587, 2017, doi: 10.1016/j.apenergy.2016.09.071.
- [24] M. Ehsani, Y. Gao, and A. Emadi, *Modern electric, hybrid electric and full cell vehicles*. Taylor & Francis Group, 2010.
- [25] K. Wipke *et al.*, "Advisor 2.0: A second generation advanced vehicle simulator for systems analysis," in "No. NREL/TP-540-25928," National Renewable Energy Laboratory, Golden, CO (US), 1999.
- [26] H. Naunheimer, B. Bertsche, J. Ryborz, and W. Novak, *Automotive transmissions: fundamentals, selection, design and application*. Springer Science & Business Media, 2010.
- [27] L. Li, X. Li, X. Wang, Y. Liu, J. Song, and X. Ran, "Transient switching control strategy from regenerative braking to anti-lock braking with a semi-brake-by-wire system," *Vehicle System Dynamics*, vol. 54, no. 2, pp. 231-257, 2016, doi: 10.1080/00423114.2015.1129059.
- [28] J. Wu, X. Wang, L. Li, C. a. Qin, and Y. Du, "Hierarchical control strategy with battery aging consideration for hybrid electric vehicle regenerative braking control," *Energy*, vol. 145, pp. 301-312, 2018, doi: 10.1016/j.energy.2017.12.138.
- [29] H. Borhan, A. Vahidi, A. M. Phillips, M. L. Kuang, I. V. Kolmanovsky, and S. Di Cairano, "MPC-Based Energy Management of a Power-Split Hybrid Electric Vehicle," *IEEE Transactions on Control Systems Technology*, vol. 20, no. 3, pp. 593-603, 2012, doi: 10.1109/tcst.2011.2134852.
- [30] Y. Cai, F. Yang, and M. G. Ouyang, "Impact of control strategy on battery degradation for a plug-in hybrid electric city bus in China," *Energy*, vol. 116, pp. 1020-1030, 2016, doi: 10.1016/j.energy.2016.09.137.
- [31] L. Raslavičius, M. Starevičius, A. Keršys, K. Pilkauskas, and A. Vilkauskas, "Performance of an all-electric vehicle under UN ECE R101 test conditions: A feasibility study for the city of Kaunas, Lithuania," *Energy*, vol. 55, pp. 436-448, 2013, doi: 10.1016/j.energy.2013.03.050.